ACS APPLIED MATERIALS & INTERFACES

Research Article

www.acsami.org

Epitaxial $LiCoO_2$ Films as a Model System for Fundamental Electrochemical Studies of Positive Electrodes

Saya Takeuchi,*[,†] Haiyan Tan,[‡,†] K. Kamala Bharathi,[†] Gery R. Stafford,[†] Jongmoon Shin,[§] Shintaro Yasui,[†,§,∥] Ichiro Takeuchi,[§] and Leonid A. Bendersky[†]

[†]Material Measurement Laboratory, National Institute of Standards and Technology, Gaithersburg, Maryland 20899, United States

[‡]Theiss Research, La Jolla, California 92037, United States

[§]Department of Materials Science and Engineering, University of Maryland, College Park, Maryland 20742, United States

[∥]Materials and Structures Laboratory, Tokyo Institute of Technology 4259-J2-19, Nagatsuta, Midori, Yokohama, 226-8503 Japan

ABSTRACT: Epitaxial $LiCoO_2$ (LCO) thin films of different orientations were fabricated by pulsed laser deposition (PLD) in order to model single-crystal behavior during electrochemical reaction. This paper demonstrates that deposition of conductive $SrRuO_3$ between a $SrTiO_3$ (STO) substrate and an LCO film allows (1) epitaxial growth of LCO with orientation determined by STO and (2) electrochemical measurements, such as cyclic voltammetry and impedance spectroscopy. Scanning transmission electron microscopy (S/TEM and SEM) has demonstrated an orientation relationship between LCO and STO of three orientations, (111), (110) and (100), and identified a LCO/electrolyte surface as consisting of two crystallographic facets of LCO, (001) and {104}. The difference in the orientation of LCO accounts for the difference in the exposed area of {104} planes to the electrolyte, where lithium ions have easy access to fast diffusion planes. The resistance for lithium ion transfer measured by electrochemical impedance spectroscopy had inverse correlation with exposed area of {104} plane measured by TEM. Chemical diffusivity of lithium ions in LCO was measured by fitting electrochemical impedance spectroscopy data to a modified Randles equivalent circuit and allowed us to determine its dependence on film orientation.

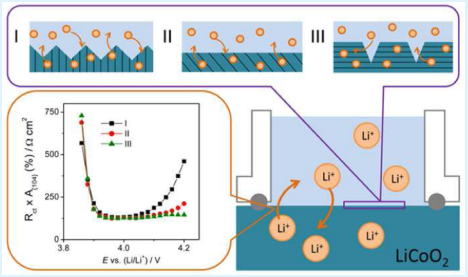

KEYWORDS: *$LiCoO_2$, epitaxial thin films, interface, orientation, transmission electron microscopy*

1. INTRODUCTION

The charge−discharge reaction of rocking-chair-type lithium ion batteries (LIB) involves complex processes of lithium ion migration between positive and negative electrodes. For example, during the charging reaction of a full cell battery, there is migration of lithium ions through the positive electrode material, lithium ion transfer from the electrode to electrolyte, migration of solvated lithium ions in the electrolyte, desolvation and transfer of lithium ions to negative electrode material, and migration of lithium ions in the negative electrode. Generally, LIB electrodes are composites consisting of a mixture of electrochemically active material and conductive media (usually carbon material), held together with binder. It is difficult to characterize performance of the active material without taking into account the other components. In the case of the positive electrode, for example, loss of interparticle electrical contact or contact with electrolyte can lead to loss of capacity,[1] which is not due to the intrinsic electrochemical property of an active material, but rather due to mechanical imperfections of a battery. To understand the nature of the electrochemical reaction and to avoid complexity of the composite electrode, it is highly advantageous to test an active material in the absence of a binder and conductive components. One of the ways to achieve this is to use a continuous thin film electrode on a conductive substrate.

$LiCoO_2$ (LCO) has been the most important and most studied positive electrode material for lithium ion batteries, and is an excellent model system for fundamental studies. There are a number of publications where LCO in the form of a thin film has been studied.[2−12] In most of the works, the studied films were polycrystalline, although preferred [001] growth orientation of LCO allowed to derive conclusions about anisotropic properties of LCO and its lithiation process.[2−5] To that end, considering a limited amount of research on oriented LCO,[13,14] in this paper, we have focused on studying epitaxial thin film LCO electrodes; the expected single orientation of LCO should allow not only better understanding of dependence of electrochemical properties on crystallographic orientation of structure and surfaces but also high quality atomic-scale electron microscopy at different stages of lithiation.

The rhombohedral $R\bar{3}m$ structure of a high temperature LCO phase that is typically used in a LIB has a layered structure consisting of an ABC framework of oxygen anions where (001) layers of Li^+ and Co^{3+} cations alternate in one direction. In this anisotropic structure, diffusion of lithium ions has been shown by first-principles calculations to be minimal across the layers

Received: December 3, 2014
Accepted: March 27, 2015
Published: March 27, 2015

DOI: 10.1021/am508512q
ACS Appl. Mater. Interfaces 2015, 7, 7901−7911

and highest along the layers;[15] e.g., it is expected that lithium ion transport is rapid for the grains with (101) and (104) surfaces, whereas it is negligible for the (001) surface,[2] and it is also reported that grain boundaries have comparable or faster lithium ion diffusion than in the LCO lattice.[4] Another reason for the kinetic dependence on orientation is the difference of charge transfer resistance at the electrode/electrolyte interface, which has been confirmed experimentally for textured polycrystalline LCO films pulse laser deposition (PLD) deposited on Pt substrates.[3] Accordingly, kinetics for charge/discharge processes should strongly depend on orientation. However, because of the films' polycrystallinity, these reports could provide only qualitative information on the lithium ion transfer at specific electrolyte/LCO interfaces, and with epitaxial films the hope is to gain more definitive answers.

One way to control LCO orientation is to utilize epitaxial growth on suitable single-crystal substrates. It is reported that $SrTiO_3$ (STO) substrates with 111, 110 and 100 surfaces induce 001, 110 and 104 out-of-plane orientations of LCO, respectively.[13,16] To make the thin film work as an electrode for measuring its electrochemical properties, there should be a highly conductive current collector, which also maintains the epitaxial growth on nonconductive STO substrates. Our recent attempts to utilize conductive Nb-doped STO (5×10^{-3} Ω cm at 300 K) as both current collector and epitaxy-inducing substrate failed to capture the electrochemical characteristics of LCO; the problem was the rectifying heterojunction between Nb-STO and LCO.[16] Suzuki et al. have demonstrated the possibility of measuring cyclic voltammogram and charge−discharge curves for $LiMn_2O_4$ films on (111) STO by using a $SrRuO_3$ (SRO) buffer layer.[17] The resistivity of SRO is reported to be $\sim 2\times 10^{-4}$ Ω cm at 300 K, which is comparable to metals,[18] and its Fermi level is reported to be 5.2 eV.[19,20] The Fermi level of LCO is 4.0 eV vs Li/Li^+,[21] from which we calculate to be 5.43 eV vs vacuum.[22,23] Thus, the band gap between SRO and LCO is 0.23 eV; this band gap is relatively small, and allows SRO to function as a current collector without rectifying the LCO/SRO interface during electrochemical measurements.

The goal of this paper is to (1) demonstrate the feasibility of making epitaxial LCO/SRO/STO films of different orientations and utilization of the SRO layer for measuring electrochemical properties of LCO; (2) demonstrate the ability to evaluate these epitaxial films using a variety of electrochemical methods. This paper is focused on measuring the electrochemical properties of the oriented LCO films, especially the transfer of lithium ions at the electrode/electrolyte interface. The studied films are in three different orientations, according to the orientations of the STO substrates and their epitaxial SRO layer. An examination of these three orientations may lead to a better understanding of the effect of anisotropy of lithium ion diffusion and charge transfer on the electrochemical behavior of the films. For quantitative evaluation of these effects, precise knowledge of the films' surface morphology and crystallography is necessary, thus a detailed cross-sectional transmission electron microscopy (TEM) analysis of the films was performed.

2. EXPERIMENTAL SECTION

2.1. Sample Preparation and Characterization. SRO (electrical conductive layer) and LCO thin films were deposited sequentially on STO substrates (square shape, approximately 0.5 × 0.5 cm) with (100), (110) and (111) surfaces using pulsed laser deposition (PLD). SRO was deposited at 650 °C and LCO was deposited at 600 °C temperature of the substrate, 200 mTorr oxygen pressure and a KrF laser (wavelength 248 nm). In this paper the samples LCO/SRO/STO (100), LCO/SRO/STO (110), LCO/SRO/STO (111) will be labeled as LCO/STO (100), LCO/STO (110) and LCO/STO (111), respectively. Extra lithium containing $Li_{1.4}CoO_2$ ceramic pellet from Toshima Co.* (*Certain commercial equipment, instruments, or materials are identified in this document. Such identification does not imply recommendation or endorsement by the National Institute of Standards and Technology, nor does it imply that the products identified are necessarily the best available for the purpose.) was employed for all the depositions. The laser repetition rate was 10 Hz and the laser energy was 100 mJ per pulse. The STO substrates were cleaned with acetone and ethanol for 15 min each in a sonicator. All the substrates were thoroughly dried with nitrogen before introducing them into the deposition chamber, which was initially evacuated to a base pressure of $\sim 4 \times 10^{-6}$ Torr. LCO and SRO targets (2.54 cm diameter) were placed on a target holder, which is placed at a distance of 6.8 cm from the substrate. Before each deposition, the targets were presputtered for 5 min to eliminate the impurities on the surface.

The films' phases and orientations were evaluated by a 4-axes Bruker D8 Discover* X-ray diffraction (XRD) instrument. Structural details were investigated by scanning transmission electron microscopy (STEM) and electron diffraction. Cross-sectional TEM studies of the films were performed from thin lamellas prepared by focus ion beam (FIB) FEI Nova 600 NanoLab*. Carbon and Pt were coated in advance on the LCO film surface to protect it against ion damage. The lamellas were milled and cleaned by Ga ions to typically 50 nm in thickness for electron transparency. High angle annular dark field (HAADF)-STEM images were acquired from the prepared lamellas using a probe corrected FEI Titan 80−300 microscope operated at 300 kV. The probe is typically corrected to 20 mrad, providing a spatial resolution of 0.1 nm. The probe convergence angle is 24 mrad, and the HAADF inner and outer collection angles are 70 and 400 mrad, respectively. Electron diffraction (ED) patterns were acquired from a selected area of 150 nm in diameter covering the LCO, SRO films and the STO substrate.

2.2. Electrochemical Measurement. Electrochemical measurements were carried out in a three-electrode cell, which is shown schematically in Figure 1. Edges of a square sample were covered with Ag paste in order to maintain electric contact to the SRO layer. The LCO/SRO/STO sample, serving as the working electrode, was attached to a Cu foil that was mechanically attached to a stainless steel current collector by pressing with an O-ring. Lithium metal was used

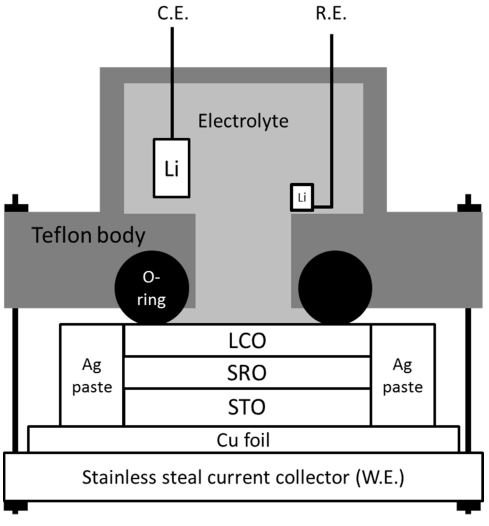

Figure 1. Schematic of an electrochemical measurement cell. W. E., C. E. and R. E. stand for working electrode, counter electrode and reference electrode, respectively.

DOI: 10.1021/am508512q
ACS Appl. Mater. Interfaces 2015, 7, 7901−7911

as counter and reference electrodes. The measured potential is referenced to Li/Li^+, unless specifically mentioned. The reaction area of a film exposed to electrolyte is determined by the Viton O-ring's size, a 0.4 cm diameter circle. The O-ring was pressed onto the sample with a Teflon holder cell, which has $\phi 2 \times 5$ mm cavity filled with electrolyte. $LiClO_4$/propylene carbonate (PC) (BASF*, battery grade) was used as an electrolyte. The $LiClO_4$/PC electrolyte was used to study LCO films with different texture,[3,6] and it is suitable for the study of epitaxial films. The concentration was varied from 1.00, 0.75, 0.50, to 0.25 mol dm^{-3}. Cyclic voltammetry was carried out with a sweep rate of 0.1 mV s^{-1}, from open circuit voltage (OCV) to 4.2 V. Impedance spectroscopy was carried out at a frequency range of 100 kHz−10 mHz. The amplitude of the potential was 10 mV. The electrode was held for 2 h at each potential in order to reach equilibrium. All electrochemical measurements were carried out in an Ar-filled glovebox at 30 °C, using a BioLogic VSP-300* potentiostat.

3. RESULTS AND DISCUSSION

3.1. XRD. Figure 2 shows the XRD patterns of LCO films grown on SRO coated STO (100), (110) and (111) substrates,

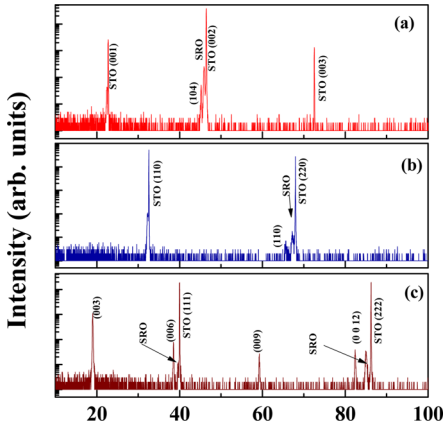

Figure 2. X-ray diffraction pattern of LCO/SRO/STO (a) (100), (b) (110) and (c) (111).

showing peaks corresponding to the (104), (110)/(108) and (00*l*) planes of the rhombohedral LCO phase, respectively, which suggests the epitaxial nature of the films. Peaks corresponding to the SRO layer are also visible and have cube-on-cube orientation with STO. Because the LCO structure has pseudo cubic arrangement of the oxygen ions sublattice similar to sublattices of both SRO and STO, the observed orientations can be understood as cube-on-cube structural relationship between all three structures.[24] Thus, {104} of LCO is equivalent to cubic (100) and parallel to the STO (100) surface; similarly, {110} and {108} of LCO are equivalent to cubic (110) and parallel to the STO (110) surface, and (001) of LCO, to cubic (111) and parallel to the STO (111) surface. Confirmation of these XRD results and derivation of the full orientation relationship can be found below in the electron diffraction analysis.

3.2. SEM and HAADF-STEM. Figure 3a illustrates the overview of the LCO/STO (100) cross-section lamella sample. The cross section image shows that SRO and LCO films have very uniform thicknesses, which are 26.5 ± 0.5 and 54 ± 1 nm, respectively. The LCO top surface is relatively flat and parallel to the STO substrate (100) plane. It demonstrates that the grooves between the grains seen in the SEM image, Figure 3b, are rather shallow (~2 nm). Figure 3c shows a selected area diffraction (SAED) pattern from a selected area in the cross

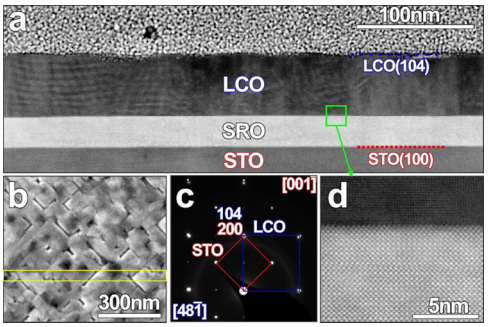

Figure 3. Characterization of the as-deposited LCO/SRO/STO (100) films (referred as LCO/STO (100) in the text) by SEM, HAADF-STEM and electron diffraction. Overviews of the films' cross sections are shown in panel a; the TEM samples were prepared by FIB from regions indicated by a yellow box in SEM images of the films' surfaces in (b). Selected area electron diffractions (SAED) include electron scattering from both film and a substrate (c). HAADF-STEM images (d) show atomically resolved LCO/SRO interfaces.

section image covering STO substrate, SRO layer and LCO film, that shows splitting of the diffraction spots to those belonging to [100] pattern of cubic STO and pseudocubic SRO, and [48-1] pattern of the rhombohedral structure of the LCO film. The enlargement of the LCO/SRO interfaces (Figure 3d) demonstrates that it is atomically sharp and epitaxial. Overall there is the following orientation relationship between the crystallographic planes parallel to the surface: LCO (104)//SRO (200)//STO (200).

Figure 4a shows a similar STEM overview image of the LCO/STO (110) cross section lifted out from a similar area

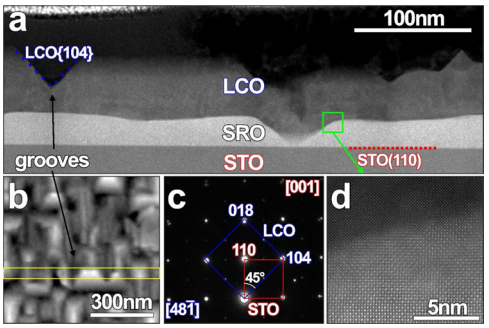

Figure 4. Characterization of the as-deposited LCO/SRO/STO(110) films(referred as LCO/STO (110) in body) by (a) HAADF-STEM at low magnification, (b) SEM, (c) electron diffraction and (d) high resolution HAADF-STEM. The {104} planes are 45° with respect to the STO(110) cut plane.

indicated in Figure 4b. The SRO and STO layers' thicknesses are 25 ± 2 and 49 ± 5 nm, respectively. Those thicknesses are very similar to that of the LCO/STO (100) sample, which means that SRO and LCO layers have similar growth rates for those two growth directions (according to different STO substrate orientations). However, compared to that of the LCO/STO (100) sample, the LCO/STO (110) film surface is not flat but has faceted grooves and a corrugated structure, and their location corresponds to intergrain boundaries. The ED patterns demonstrate that the films mainly have a single orientation and grow epitaxially to the STO substrate judging from the small spot split (Figure 4c). The epitaxial relationship is actually the same as that for the LCO/STO (100) samples

DOI: 10.1021/am508512q
ACS Appl. Mater. Interfaces 2015, 7, 7901−7911

but with all crystals rotated 45° to match LCO (018)//SRO (110)//STO (110) on film growth direction. Although the SRO/STO interface is still sharp and atomically flat (not shown here) and the LCO/SRO interface is mainly parallel to the STO (110) plane, due to the formation of grooves during the SRO growth, the LCO/SRO interface in some regions is not flat and atomically sharp, as indicated in Figure 4d. Despite this broadened interface, the crystal orientation of the STO substrate has been nicely transferred to the top LCO film.

The overview of the LCO/STO (111) cross section lamella sample shows that its SRO and LCO layers have a flat interface (Figure 5a). The LCO surface is predominately flat, with

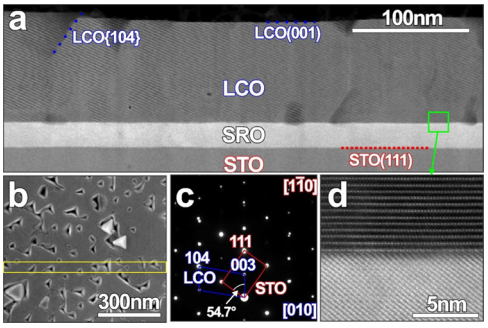

Figure 5. Characterization of the as-deposited LCO/SRO/STO (111) films (referred as LCO/STO (111) in body) by (a) STEM overview, (b) SEM, (c) electron diffraction and (d) high resolution HAADF-STEM. The {104} planes are 54.7 ° with respect to the horizontal STO (111) cut plane.

crystallographic (001) plane, but also with occasional faceted grooves. According to the SEM image, Figure 5b, the surface consists of triangular islands or holes with faceted surfaces that are {104} planes. SRO and LCO layers' thicknesses are 21.6 ± 0.5 and 92 ± 3 nm, respectively, which is almost 2 times that of LCO (001) and LCO (110) (Table 1). The ED pattern is

Table 1. LCO/STO Films and LCO Exposed Planes and Its Lithium Ion Transfer Active Surface Areas Comparing Physical Horizontal Surface

	STO surface cut	SRO thickness (nm)	LCO thickness (nm)	LCO exposed planes	active surface {104} area (%)
LCO/STO (100)	(100)	26.5 ± 0.5	54 ± 1	{104}	100
LCO/STO (110)	(110)	25 ± 2	49 ± 5	{104}, {001}	141.4
LCO/STO (111)	(111)	21.6 ± 0.5	92 ± 3	{104}, {001}	54.4

shown in Figure 5c, where the STO [110] pattern with (111) plane parallel to the substrate's surface, and the pattern of rhombohedral LCO at [100] direction are recognized. The crystal orientation between layers is LCO (003)//SRO (111)//STO (111). Figure 5d shows that the LCO/SRO interface is atomically sharp, which provides the good structural quality of these samples.

One of the reasons to work with epitaxial LCO films of different orientations was verification of the proposition that the (001) LCO plane is not active for lithium ion transfer. However, the desired rhombohedral LCO phase is formed by an island growth mechanism that creates low energy facets on the surface. Coalescence of the islands during growth does not completely eliminate the facets, and thus the films' surface are composed of a combination of the growth facets. Although films with a single crystallographic surface were not achieved, the surface area of the lithium ion transfer active surfaces with exposed terminations of (001) planes and their fraction is straightforward to estimate from the SEM and cross-sectional TEM images.

Analysis of the images demonstrates that the LCO films' exposed surfaces are a single (001) and a family of three {104} surfaces (for the $R\bar{3}m$ trigonal symmetry) (for details, see ref 16). This observation agrees with the theoretical calculation by Kramer and Ceder, which shows that these two family planes are the lowest energy planes.[25] During deposition, there is a competition between growth direction (and corresponding planes) established by orientation relationship with a particular substrate and the low-energy facets. The LCO/STO (100) sample shows a very flat surface (Figure 3a), which means that the surface exposed to electrolyte is composed entirely of the active {10-4} surface. The LCO/STO (110) samples have a corrugated surface (Figure 4b), with predominately {104} surface planes inclined 45° with respect to the STO 110 cut plane (Figure 4c). Thus, the surface area taken by active {10-4} facets is 100%/cos (45°) = 141.4% of the nominal surface. This lithium ion transfer active surface is estimated to be almost 50% larger than that of the LCO/STO (100) films. Measurements of the SEM images for LCO/STO (111) show that 68.6% of the projected sample's surface is flat (001) plane, and the other 31.4% belongs to triangulated grooves or holes (separated by thin gray lines in Figure 5b). The grooves' surfaces are {10-4} facets, which are inclined 54.7° with respect to the STO (111) cut plane (Figure 5c). The average depth of the grooves is about 30 nm, and the average side of the groove is about 50 nm; these dimensions make almost all grooves inverted triangular pyramids. With this estimation, the active {10-4} surface area is approximately 31.4%/cos (54.7°) = 54.4%. Thus, for the same geometric area exposed to the electrolyte (determined by the O-ring size), the lithium ion transfer active surface with is 100%, 140% and <50% for LCO/STO (100), LCO/STO (110) and LCO/STO (111), respectively.

3.3. Electrochemical Measurement. *3.3.1. Cyclic Voltammetry (CV).* Figure 6a–c shows cyclic voltammograms obtained from three films, (a) LCO/STO (100), (b) LCO/STO (110) and (c) LCO/STO (111). There is a strong similarity between these three scans, both in the reversibility, position and number of redox peaks. For oxidation peaks in the scan from 3.2 to 4.2 V (deintercalation, or removal of lithium ions from LCO), one can observe three peaks: the highest peak appears at 3.94 V, followed by smaller, broader peaks around 4.06 and 4.18 V. These peaks are similar to those typically observed for LCO powder and can be interpreted by a sequence of phase transitions resulting from removal of lithium ions, as reported by Reimers et al.[26] No voltammetric waves are observed in control experiments utilizing SRO/STO electrodes without the LCO film. In contrast, a large continuous anodic current approaching 100 μA cm^{-2} is measured, which suggests that SRO would dominate the electrochemical response if exposed to the electrolyte. This further supports our assessment that all the peaks observed in Figure 6 are due to the electrochemical reaction of LCO.

These results show that deintercalation and intercalation of lithium ions takes place at the same potentials for all three

DOI: 10.1021/am508512q
ACS Appl. Mater. Interfaces 2015, 7, 7901–7911

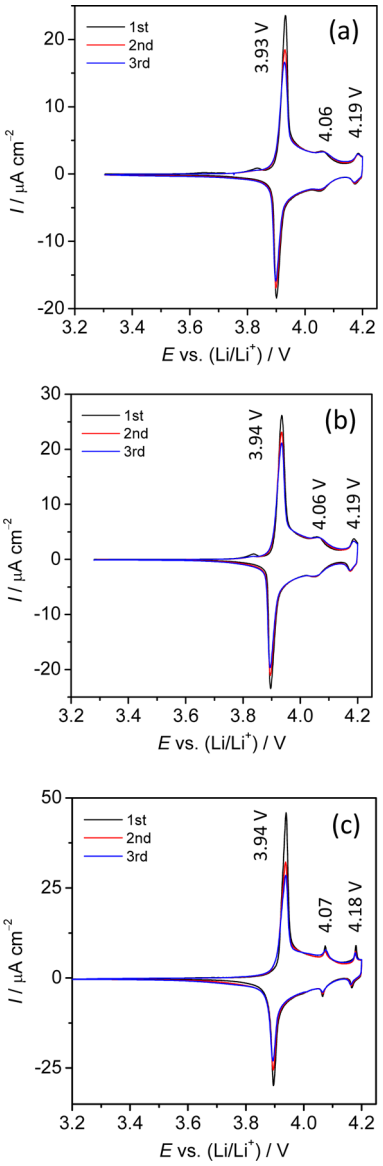

Figure 6. Cyclic voltammograms of LCO/SRO/STO (a) LCO/SRO/STO (100), (b) LCO/SRO/STO (110) and (c) LCO/SRO/STO (111) in 1 mol dm^{-3} $LiClO_4$/PC.

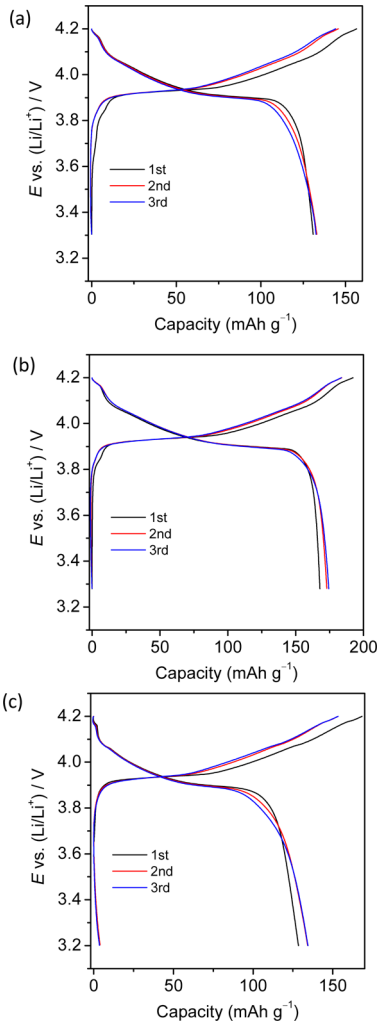

Figure 7. Capacity vs E obtained from cyclic voltammograms from applied current. LCO/SRO/STO (a) LCO/SRO/STO (100), (b) LCO/SRO/STO (110) and (c) LCO/SRO/STO (111).

orientations with comparable levels of extracted/inserted lithium, which is contrary to the intuitive expectation that LCO/STO (111) is passive for lithium ion transfer because the LCO (001) film surface prevents access of lithium ion to high-diffusivity channels. With the help of detailed TEM analysis this discrepancy can be understood as follows: Even though the orientation of the LCO phase is fixed, because of the lower symmetry and island mode of growth of the rhombohedral phase, the films are not a single crystal with a single crystallographic surface but consist of faceted domains. In particular, the LCO/STO (111) has not only LCO (001) planes but a certain, measurable fraction of {10-4} planes with easy access for lithium ions to the high-diffusivity channels.

Figure 7a–c shows capacity (mAh g^{-1}) vs E of (a) LCO/STO (100), (b) LCO/STO (110) and (c) LCO/STO (111) obtained by integrating the current of the cyclic voltammograms in Figure 6a–c. The expected capacity of our thin film can be calculated from molar volume of LCO V_m (19.56 cm^3 mol^{-1}), molar mass of LCO (97.87 g mol^{-1}), exposed area of electrode (0.13 cm^2) and thickness of LCO (50–100 nm) from Table 1, and compared to the theoretical capacity of stoichiometric LCO (272 mAh g^{-1}). For all three orientations in Figure 7, a large plateau is observed around 3.94 V, followed by small plateaus around 4.06 and 4.19 V. The plateau corresponds to peak positions observed in the cyclic voltammograms in Figure 6. The largest plateau at 3.94 V is due to a two phase coexistence.[26,27] It was reported that a monoclinic phase exists around $Li_{0.5}CoO_2$[26,27] where hexagonal phases exist at higher and lower lithium content than $Li_{0.5}CoO_2$.[27] By comparing our cyclic voltammograms to those in the literature, e.g., ref 26, the small peaks at 4.06 and 4.19 V in Figure 6 are interpreted as phase transitions from hexagonal to monoclinic at 4.06 V and monoclinic to hexagonal at 4.19 V. The total charge passed at this potential range for (a) LCO/STO (100) and (c) LCO/STO (111) is approximately 136 mAh g^{-1}, which is half of theoretical capacity. Hence, these two orientations show capacitance close to the theoretical of $Li_{0.5}CoO_2$. We believe that (b) LCO/STO (110) shows higher capacity than the other two because of greater uncertainty in the thickness of LCO/STO (110), which shows pronounced surface variations (see Table 1 and Figure 4).

A capacity loss in the first cycle was observed to be higher than in the second and third cycles, and it was observed for all

DOI: 10.1021/am508512q
ACS Appl. Mater. Interfaces 2015, 7, 7901–7911

three orientations. This can be attributed to an irreversible oxidation reaction that leads to surface film formation and/or deterioration of LCO during the measurement. The irreversible oxidation around 3.8 V can be clearly seen in (a) LCO/STO (100) and (b) LCO/STO (110) first cycles, although it is not observed in (c) LCO/STO (111). Indeed, surface film formation on LCO in organic solvents is reported by Matsui et al. near this potential.[28] Surface film formation was more prominent in the first cycle than the following cycles, indicating the fresh surface of LCO is more reactive with solvent than after cycling. A shoulder at around 3.9 V in reduction curves appears to diminish as cycle number increases. This indicates a possible deterioration of the LCO structure during cycling.

Because the theoretical capacity and the capacity obtained from cyclic voltammetry are similar, we can conclude that the entire LCO film in contact with electrolyte (inside the O-ring) was reacted; thus for the scan rate of 0.1 mV s^{-1}, we can assume that the CV was obtained under close to equilibrium conditions.

3.3.2. Impedance Spectroscopy. Figure 8 shows the Nyquist plots for the (a) LCO/STO (100), (b) LCO/STO (110) and (c) LCO/STO (111) films at various steady state potentials. The modified Randles equivalent circuit shown in Figure 9 was

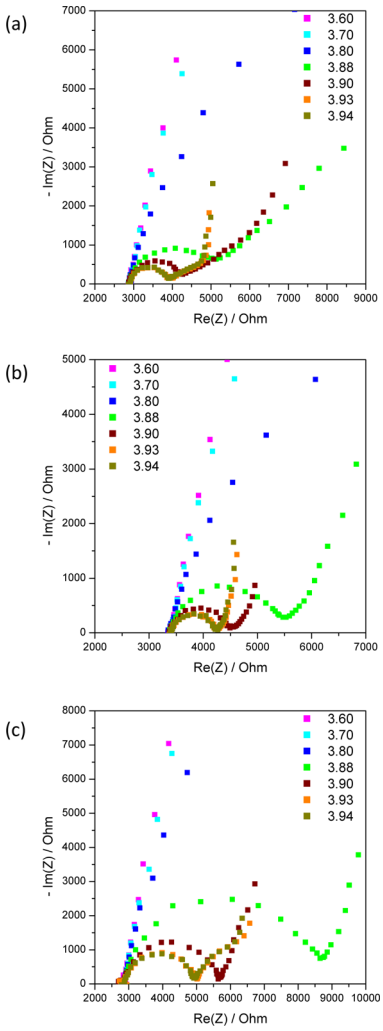

Figure 8. Nyquist plot of LCO/SRO/STO (a) 100, (b) 110 and (c) 111 in 1 mol dm^{-3} $LiClO_4$/PC. Potentials were 3.60, 3.70, 3.80, 3.88, 3.90, 3.93 and 3.94 V.

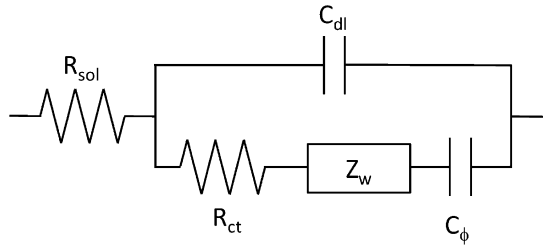

Figure 9. Equivalent circuit that is used for analysis of impedance spectra. R_{sol}: solution resistance of electrolyte. C_{dl}: double layer capacitance. R_{ct}: resistance of lithium ion transfer. Z_w: diffusion of lithium ion in the electrode (Warburg impedance). C_ϕ: pseudocapacitance for nonideal finite diffusion.

used to model this impedance behavior;[23] the circuit components are R_{sol} for the solution resistance of the electrolyte, C_{dl} for the double layer capacitance, R_{ct} for the charge transfer resistance for lithium ion deintercalation/intercalation at the LCO/electrolyte interface and Z_w for the Warburg impedance that reflects lithium ion diffusion in LCO. We have also added C_ϕ as a pseudocapacitance for nonideal finite diffusion, which has been used by Funabiki et al. for graphite.[29] In the potential range that LCO is not active for lithium ion deintercalation/intercalation, the equivalent circuit can be represented by a series R_{sol} and C_{dl}. R_{sol} appears as an intercept on the real axis at high frequency, when the impedance of the double layer is small compared to that of charge transfer. The semicircle that is observed at more positive potential represents the transfer of lithium ion from/into LCO. The diameter of the semicircle on the real axis is equivalent to R_{ct}. Assuming semi-infinite diffusion, Z_w should appear as a 45° straight line on the Nyquist plot. The Warburg coefficient σ (Ω cm^2 $s^{-1/2}$) is correlated as

$$Z_w = (1 - \sqrt{j})\sigma\omega^{-1/2} \quad (1)$$

where ω is the radial frequency. The Warburg coefficient can be used to evaluate lithium ion chemical diffusion in LCO. The pseudocapacitance C_ϕ was employed in order to account for finite capacity, which limits the charge transfer along the Faradaic leg of the equivalent circuit. The characteristics of this element on the Nyquist plot is a transition of the Warburg response from 45° to a vertical line that is parallel to the imaginary axis. The impedance response shown in Figure 8 consists of a near vertical line at $Z' \approx 3000$ Ω at potentials from 3.60 to 3.80 V for all three films, depicting the expected series $R_{sol}-C_{dl}$ behavior in this potential region. This is consistent with the voltammetry, which shows only capacitive behavior at these potentials. For all three films, the semicircles appear at potentials >3.88 V. These values of R_{ct} obtained from the semicircles become smaller with increasing potential and reach a minimum value around 3.94 V, corresponding to the primary voltammetric peak in Figure 6. This behavior suggests that the semicircles in the Nyquists plots can be attributed to lithium ion deintercalation/intercalation at about 3.94 V.

To confirm this, the concentration of $LiClO_4$ was varied from 1.00 to 0.25 mol dm^{-3} to establish the dependence of R_{ct} on the lithium ion concentration in electrolyte. The experimental results for LCO/STO (110) showing dependence between $1/R_{ct}$ and lithium ion concentration C are presented in Figure 10. The dependence is nearly linear and can be explained as described below.

The exchange current i_0 can be written as

DOI: 10.1021/am508512q
ACS Appl. Mater. Interfaces 2015, 7, 7901−7911

$$i_0 = nFAk^0C \quad (2)$$

where n is the number of electrons involved in the formal reaction, F is the Faraday constant (96 500 C mol^{-1}), A is the electrode area, k^0 is the standard rate constant and C is the concentration of electroactive species in the electrolyte. Because the electrode was equilibrated at each potential, and the amplitude of the ac potential was small, the Butler–Volmer equation can be written as

$$i = -i_0\eta nF/RT \quad (3)$$

where i is the steady state current, η is the overpotential, R is the gas constant and T is the absolute temperature.[23] Because $-\eta/i$ is equal to the charge transfer resistance R_{ct}, eq 3 can be expressed as

$$R_{ct} = RT/nFi_0 \quad (4)$$

From eqs 2 and 4, the linear dependence of C and $1/R_{ct}$ is obtained as

$$C = RT/(nF^2Ak^0)1/R_{ct} \quad (5)$$

In this paper, C is the lithium ion concentration in the electrolyte and R_{ct} is the charge transfer resistance for lithium intercalation/deintercalation. Hence, when the semicircle is due to lithium ion transfer at the LCO interface, the $1/R_{ct}$ vs $LiClO_4$ concentration dependence should be linear, as shown in Figure 10. The same trend was also observed for LCO/STO (100) and (111).

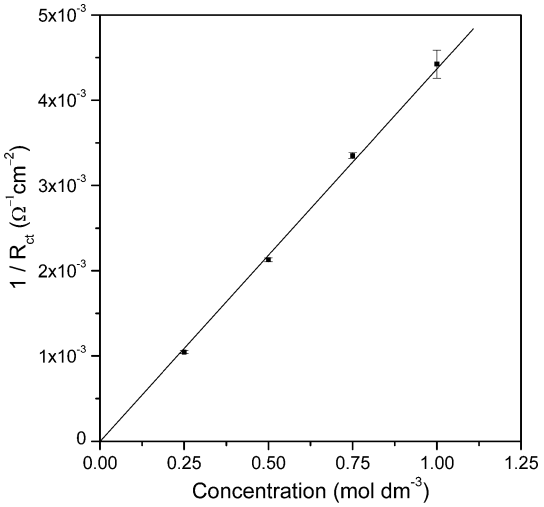

Figure 10. Dependence of $1/R_{ct}$ on concentration of LCO/STO (110). Error bars are from standard deviation of R_{ct} from fitting to modified Randles circuit.

The impedance data in Figure 8 was fitted to the equivalent circuit in Figure 9 using commercial software (EC-lab* from BioLogic) in order to determine the potential dependence of the various circuit elements. Selected impedance data and the corresponding fits of LCO/STO (110) at 3.88, 3.94 and 4.20 V are shown in Figure 11. Nearly all of the essential features of the Nyquist plot are captured by the fitting procedure; i.e., the semicircle representing the lithium ion charge transfer resistance, the Warburg region (45°) where lithium ion diffusion in LCO is rate determining, and finally the low frequency region where limited charge capacity curtails the charge transfer reaction.

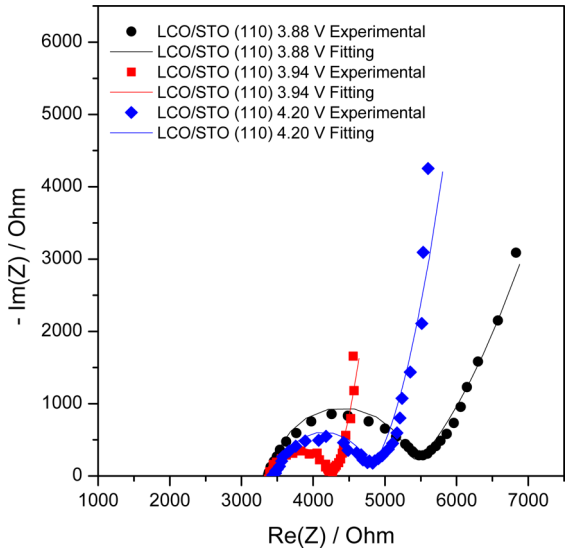

Figure 11. Experimental data of impedance spectroscopy and fitting of LCO/STO (110) at 3.88, 3.94 and 4.20 V.

We will now examine the values of the various circuit elements in detail. The value of R_{sol} obtained from the fit is typically about 3000 Ω in 1.0 mol dm^{-3} $LiClO_4$/PC. The resistance is attributed to solution resistance (R_{sol}) of electrolyte, not to the interfacial resistance of LCO/SRO nor SRO contact to the current collector. To confirm this, the conductivity of 1.0 mol dm^{-3} $LiClO_4$/PC electrolyte was measured using a two electrode conductivity cell with Pt black electrodes and cell constant of 99.7 ± 0.95 m^{-1}. The conductivity was measured to be 4.83 mS cm^{-1}. Considering the cell geometry shown in Figure 1, and assuming that R_{sol} is due to the $\phi 2 \times 5$ mm electrolyte cavity between the working and reference electrodes, we calculate an R_{sol} value of 3296 Ω based on the 4.83 mS cm^{-1} conductance value. This was also confirmed experimentally by replacing the LCO/SRO/STO thin film electrode with Cu foil and repeating the impedance measurement in the double layer region for Cu. R_{sol} values of 3000 Ω were obtained in this configuration as well, confirming that R_{sol} is primarily due to solution resistance and that the LCO/SRO interface and electric contact using Ag paste do not contribute significant resistance to the measurement.

The double layer capacitance provides information about the LCO/electrolyte interface. Figure 12 shows the potential dependence of C_{dl} for the three different orientations. The experimentally obtained C_{dl} values are normalized to the geometric O-ring area of 0.13 cm^2. For LCO/STO (100), the C_{dl} value was about 6 μF cm^{-2}, LCO/STO (111) was about 10 μF cm^{-2} and LCO/STO (110) was about 18 μF cm^{-2}. These variations in C_{dl} values can be explained by systematic variations in total faceted surface area, as was observed in Figures 3–5. The value for C_{dl} stays constant with voltage for all three orientations until about 4.05 V, at which point a slight increase in C_{dl} is observed for LCO/STO (110). The relatively constant C_{dl} suggests that the surface area (and perhaps morphology) remain unaltered during the oxidation of LCO. This is consistent with the stable charge–discharge curves in Figure 7, where the experimentally obtained capacity is in good agreement with theoretical capacity.

Figure 13a shows the variation of R_{ct} with potential for LCO/STO (100), (110) and (111). In the potential range of 3.9 to about 4.1 V, the value of R_{ct} was relatively constant and

DOI: 10.1021/am508512q
ACS Appl. Mater. Interfaces 2015, 7, 7901–7911

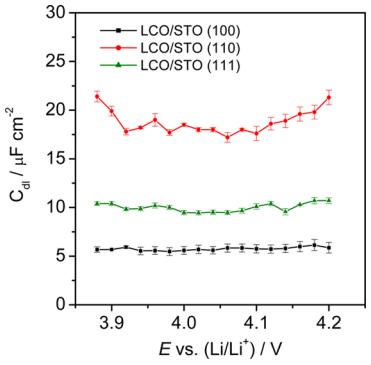

Figure 12. Variation of C_{dl} for LCO/STO (100), (110) and (111). Error bars are equivalent to standard deviation of C_{dl} from fitting to modified Randles circuit.

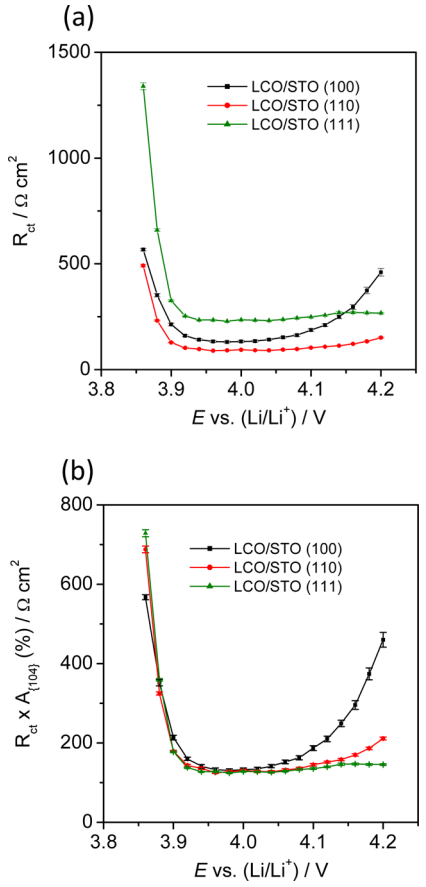

Figure 13. Dependence of R_{ct} on potential for LCO/STO (100), (110) and (111). Error bars are standard deviation of R_{ct} from fitting to modified Randles circuit, normalized with O-ring area. (a) R_{ct} obtained by fitting with the equivalent circuit shown in Figure 9. (b) Normalized with lithium ion transfer active surface area {104}. Values for the lithium ion transfer active surface area are from Table 1.

decreased in the order of LCO/STO (111) > LCO/STO (100) > LCO/STO (110). For potentials of 4.1 V and above, R_{ct} increased for LCO/STO (100) and (110), and remained essentially constant for LCO/STO (111). The values of R_{ct} in Figure 13a are normalized to the geometric electrode area that is in contact with electrolyte. However, the rate of lithium ion transfer at the LCO/electrolyte interface is determined by the surface area that is active to lithium ion transfer. The active surfaces of LCO are those where lithium ion can directly access (001) lithium layers of high diffusivity, and activity of these surfaces is proportional to the density of active sites, which is the density of intersection between (*hkl*) surface plane and (001) (proportional to sin α, where α is an angle between normal to (*hkl*) and (001)). For faceted corrugated surfaces, all the active surfaces can be measured and normalized to their activity. In our study, according to SEM and cross-sectional TEM, the films' surfaces consist of only active {104} and inactive (001) surfaces. With the assumption that only active surface contribute to the ion transfer (and thus to R_{ct}), we estimate the active area A from SEM and TEM areas of {104} lithium ion transfer active surfaces as $A_{100}/A_{100} = 1$, $A_{110}/A_{100} = 1.4$ and $A_{111}/A_{100} = 0.5$ for LCO/STO (100), (110) and (111), respectively. Figure 13b shows the same R_{ct} data as in Figure 13a, this time normalized to the estimated {104} surface area. In the potential range of 3.9–4.0 V, R_{ct} is identical for all three orientations. This suggests that the {104} plane is the primary lithium ion transfer active surface for the lithium ion charge transfer reaction at the LCO/electrolyte interface.

Figure 13b also indicates that as the potential is increased to 4.2 V, R_{ct} increases for LCO/STO (100) and LCO/STO (110), while it remains essentially constant for LCO/STO (111). This increase in R_{ct} might possibly be due to surface film formation at the LCO/electrolyte interface, as has been suggested in recent work by Hirayama et al. In that work, $LiNi_{0.8}Co_{0.2}O_2$ epitaxial thin film electrodes grown on STO (110) were subject to surface film formation, whereas $LiNi_{0.8}Co_{0.2}O_2$ grown on STO (111) were not.[30] Although surface film formation could restrict the transfer of lithium ions at an LCO active site, and, in turn, increase the value in R_{ct}, one would also expect it to directly impact the double layer capacitance. However, the values of C_{dl} plotted in Figure 12 for LCO/STO (100) are constant throughout the measured potential range, suggesting that the observed increase in R_{ct} with potential might be caused by other factors.

We now examine the influence of the LCO's anisotropy on the lithium ion diffusion in the oriented films. Values of the chemical diffusion coefficient of lithium ions reported in the literature vary significantly from 10^{-13} to 10^{-7} cm^2 s^{-1}.[31−35] This large variation is due to a number of factors, including uncertainty in the electrode thickness and undefined surface morphology/orientation; these uncertainties should be reduced for the epitaxial thin films. Referring to the Figure 9 equivalent circuit, lithium ion diffusion in LCO is accounted for by the Warburg impedance (Z_w) through the Warburg coefficient σ, which is plotted in Figure 14a for the three film orientations as a function of potential. The Warburg coefficient is seen to increase with increasing potential, reflecting the corresponding increase in the diffusional impedance Z_w. The chemical diffusion coefficient for lithium ion can be calculated from the Warburg coefficient from the following expression[35,36]

$$D = 1/2[(V_m/nF\sigma)(dE/dx)]^2 \quad (6)$$

where x is a value that represents chemical composition as in Li_xCoO_2 and dE/dx is the derivative of the Li_xCoO_2 charge curve. In our experiments, dE/dx was obtained from oxidation curves in cyclic voltammetry, under the assumption that the LCO electrode was at equilibrium over the entire range of potentials. A value of $x = 0.5$ is set for the monoclinic phase in the potential range of 4.06–4.19 V.[26,27]

Figure 14b shows plots of D vs E for LCO/STO (100), (110) and (111). It is interesting to note that although σ shows a steady increase with potential, this is not reflected in the

DOI: 10.1021/am508512q
ACS Appl. Mater. Interfaces 2015, 7, 7901−7911

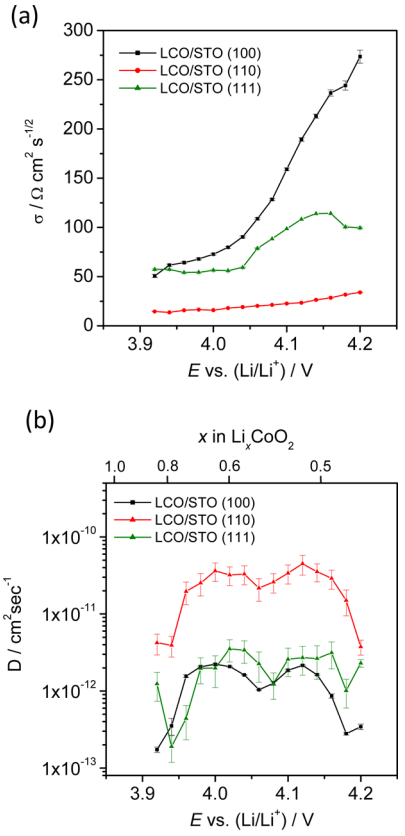

Figure 14. (a) σ vs E and (b) D vs E of LCO/STO (100), (110) and (111). Error bars are (a) standard deviation of σ and (b) calculated from propagation of standard deviation of dE/dx and σ from fitting to modified Randles circuit. x in Li_xCoO_2 is obtained by fixing $x = 0.5$ at the potential with minimum current density between 4.06 and 4.19 V peaks in CV of LCO/STO (100).

diffusion coefficient due to the offsetting contributions of dE/dx. The value of D varies from 10^{-13} to 10^{-10} cm^2 s^{-1}. For all three orientations, D increases in the early stages of LCO oxidation, remains reasonably constant over a wide range of potentials and then decreases as x (in Li_xCoO_2) approaches a value of 0.5. This behavior is fairly consistent with first-principles calculations[15] as well as experimental results that appear in the literature.[35,37−39] The decrease at the more positive potentials has been attributed to a higher activation energy associated with lithium jumps in ordered $Li_{0.5}CoO_2$.[15] It was further noted that the magnitude of the decrease in D is very sensitive to degree of order in the $Li_{0.5}CoO_2$.[38]

The results in Figure 14b also show that the chemical diffusion coefficient is appreciably higher for LCO/STO (110) than for LCO/STO (100) and (111). According to theoretical studies, lithium diffusion occurs by way of a divacancy mechanism.[15,40,41] As a consequence, the chemical diffusion coefficient can be influenced by several factors, including the vacancy site concentration available for lithium ions, the activation barrier for lithium ion migration and the thermodynamic factor, which is the deviation from ideality of the lithium chemical potential.[15,39] In addition to these intrinsic factors, it has also been suggested that lithium ion diffusion in grain boundaries may be a viable transport mechanism.[4] However, because the films examined here only contain coherent twin boundaries that do not have structural free volume, their contribution to enhanced diffusion should be minimal. Although electrochemical measurements provide useful kinetic information, they only reveal the average properties of the film. A more detailed structural analysis will be required to explain the variations in the chemical diffusion coefficients shown in Figure 14b. This is the focus of our current research, and the results will be reported elsewhere.

CONCLUSIONS

1. Epitaxial LCO films in three orientations on STO substrates with (100), (110) and (111) surfaces covered with a 25 nm thick layer of SRO were prepared by PLD. Although the films have a single orientation relationship with the substrate, the lower symmetry of the rhombohedral LCO phase with respect to the cubic STO results in a domain structure of the films and correspondingly the faceted surfaces. Nevertheless, the well-characterized surfaces allow estimating the lithium ion transfer active surface area accessible for easy transfer of lithium ions into/from electrolyte.

2. It was demonstrated that the SRO conductive layer does not disrupt epitaxial thin film growth of LCO and serves as a reliable current collector for electrochemical measurements such as cyclic voltammetry and electrochemical impedance spectroscopy.

3. Cyclic voltammograms of the films with different orientations were similar to each other, and had the same characteristics of one major (3.94 V) and two minor (4.07 and 4.19 V) redox peaks as bulk LCO. We have found that lithium ion transfer active surface area measured by TEM/SEM, which are the (104) facets of the LCO surface, and the lithium ion transfer active surface area obtained from electrochemical measurements are in good accordance, which means that the LCO (104) surface is primarily responsible for lithium ion transfer at the LCO/electrolyte interface.

4. By using a modified Randles circuit, the variation of lithium ion transfer resistance (R_{ct}) and double layer capacitance (C_{dl}) with applied potential were estimated. It was found that R_{ct} increases as potential goes above 4.1 V for LCO (100) and LCO (110), but R_{ct} remained constant for LCO (111). This result suggests the formation of a surface film, which takes place more readily on LCO/STO (100) and (110) and hinders lithium ion transfer at LCO/electrolyte interface. The chemical diffusion coefficient D, obtained from Warburg impedance (Z_w) ranged from 10^{-13} to 10^{-10} cm^2 s^{-1}. The chemical diffusion coefficient was higher for LCO/STO (110) compared to LCO/STO (100) and (111).

AUTHOR INFORMATION

Corresponding Author

*S. Takeuchi. Phone: +1-301-975-8366. E-mail: saya.takeuchi@nist.gov.

Notes

The authors declare no competing financial interest.

ACKNOWLEDGMENTS

Dr. Nancy Dudney from Oak Ridge National Laboratory is acknowledged for useful suggestions and comments. H.T. acknowledges support from the U.S. Department of Commerce, National Institute of Standards and Technology under financial assistance awards 70NANB14H027 and 70NANB15H025.

DOI: 10.1021/am508512q
ACS Appl. Mater. Interfaces 2015, 7, 7901−7911

REFERENCES

(1) *Lithium Ion Batteries, Fundamentals and Performance*; Wakihara, M., Yamamoto, O., Eds.; Kodansha: Tokyo, Japan, 1998.

(2) Bates, J. B.; Dudney, N. J.; Neudecker, B. J.; Hart, F. X.; Jun, H. P.; Hackney, S. A. Preffered Orientation of Polycrystalline $LiCoO_2$ Films. *J. Electrochem. Soc.* **2000**, *147*, 59−70.

(3) Yamada, I.; Iriyama, Y.; Abe, T.; Ogumi, Z. Lithium-Ion Transfer on a Li_xCoO_2 Thin Film Electrode Prepared by Pulsed Laser Deposition − Effect of Orientation-. *J. Power Sources* **2007**, *172*, 933−937.

(4) Xia, H.; Lu, L. Texture Effect on the Electrochemical Properties of $LiCoO_2$ Thin Films Prepared by PLD. *Electrochim. Acta* **2007**, *52*, 7014−7021.

(5) Bouwman, P. J.; Boukamp, B. A.; Bouwmeester, H. J. M.; Wondergem, H. J.; Notten, P. H. L. Structural Analysis of Submicrometer $LiCoO_2$ Films. *J. Electrochem. Soc.* **2001**, *148*, A311−A317.

(6) Lee, J.-K.; Lee, S.-J.; Baik, H.-K.; Lee, H.-Y.; Jang, S.-W.; Lee, S.-M. Substrate Effect on the Microstructure and Electrochemical Properties in the Depositions of a Thin Film $LiCoO_2$ Electrolyte. *Electrochem. Solid-State Lett.* **1999**, *2*, 512−515.

(7) Antaya, M.; Reimers, J. N.; Li, W.; Dahn, J. R. Preparation and Characterization of $LiCoO_2$ Thin Films by Laser Ablation Deposition. *J. Electrochem. Soc.* **1993**, *140*, 575−578.

(8) Perkins, J. D.; Bahn, C. S.; Parilla, P. A.; McGraw, J. M.; Fu, M. L.; Duncan, M.; Yu, Y.; Ginley, D. S. $LiCoO_2$ and $LiCo_{1-x}Al_xO_2$ Thin Film Cathodes Grown by Pulsed Laser Ablation. *J. Power Sources* **1999**, *81*, 675−679.

(9) Iriyama, Y.; Inaba, M.; Abe, T.; Ogumi, Z. Preparation of c-Axis Oriented Thin Films of $LiCoO_2$ by Pulsed Laser Deposition and Their Electrochemical Properties. *J. Power Sources* **2001**, *94*, 175−182.

(10) Tang, S. B.; Lu, L.; Lai, M. O. Characterization of a $LiCoO_2$ Thin Film Cathode Grown by Pulsed Laser Deposition. *Philos. Mag.* **2005**, *85*, 2831−2842.

(11) Park, H.-Y.; Nam, S.-C.; Lim, Y.-C.; Choi, K.-G.; Lee, K.-C.; Park, G.-B.; Kim, H.-P.; Cho, S.-B. Influence of Sputtering Gas Pressure on the $LiCoO_2$ Thin Film Cathode Post-annealed at 400 °C. *Korean J. Chem. Eng.* **2006**, *23*, 832−837.

(12) Tang, S. B.; Lu, L.; Lai, M. O. Thin Film Microbatteries Prepared by Pulsed Laser Deposition. *J. Korean Phys. Soc.* **2007**, *51*, 1055−1062.

(13) Hirayama, M.; Sonoyama, N.; Abe, T.; Minoura, M.; Ito, M.; Mori, D.; Yamada, A.; Kanno, R.; Terashima, T.; Takano, M.; Tamura, K.; Mizuki, J. Characterization of Electrode/Electrolyte Interface for Lithium Batteries Using in Situ Synchrotoron X-ray Reflectometry − A New Experimental Technique for $LiCoO_2$ Model Electrode. *J. Power Sources* **2007**, *168*, 493−500.

(14) Ohnishi, T.; Takada, K. High-Rate Growth of High-Crystallinity $LiCoO_2$ Epitaxial Thin Films by Pulsed Laser Deposition. *Appl. Phys. Express* **2012**, *5*, 055502−1−055502−3.

(15) Van der Ven, A.; Ceder, G. Lithium Diffusion in Layered Li_xCoO_2. *Electrochem. Solid-State Lett.* **2000**, *3*, 301−304.

(16) Li, Z.; Yasui, S.; Takeuchi, S.; Creuziger, A.; Herzing, A.; Maruyama. S.; Takeuchi, I.; Bendersky, L. A. Structural Study of Epitaxial $LiCoO_2$ Films Grown by PLD on Single Crystal $SrTiO_3$ Substrates. *Thin Solid Films*, submitted.

(17) Suzuki, K.; Kim, K.; Taminato, S.; Hirayama, M.; Kanno, R. Fabrication and Electrochemical Properties of $LiMn_2O_4/SrRuO_3$ Multi-layer Epitaxial Thin Film Electrodes. *J. Power Sources* **2013**, *226*, 340−345.

(18) Ohnishi, T.; Takeda, K. Epitaxial Thin-Film Growth of $SrRuO_3$, $Sr_3Ru_2O_7$, and Sr_2RuO_4 from a $SrRuO_3$ Target by Pulsed Laser Deposition. *Appl. Phys. Express* **2011**, *4*, 025501-1−025501-3.

(19) Hartmann, A. J.; Neilson, M.; Lamb, R. N.; Watanabe, K.; Scott, J. F. Ruthenium Oxide and Strontium Ruthenate Electrodes for Ferroelectric Thin-Films Capacitors. *Appl. Phys. A: Mater. Sci. Process.* **2000**, *70*, 239−242.

(20) Fang, X.; Kobayashi, T. Study of Pulsed Laser Deposition of RuO_2 and $SrRuO_3$ Thin Films. *Appl. Phys. A: Mater. Sci. Process.* **1999**, *69*, S587−S590.

(21) Goodenough, J. B.; Kim, Y. Challenges for Rechargeable Li Batteries. *Chem. Mater.* **2010**, *22*, 587−603.

(22) Morrison, S. R. *Electrochemistry at Semiconductor and Oxidized Metal Electrodes*; Plenum Press: New York, NY, 1980.

(23) Bard, A. J.; Faulkner, L. R. *Electrochemical Methods Fundamentals and Applications*, 2nd ed.; John Wiley & Sons, Inc.: New York, NY, 2001.

(24) Nishino, K.; Ohnishi, T.; Akatsuka, K.; Takada, K. Cyristal Orientation of Epitaxial $LiCoO_2$ Films Grown on $SrTiO_3$ Substrates. *J. Power Sources* **2014**, *247*, 687−691.

(25) Kramer, D.; Ceder, G. Tailoring the Morphology of $LiCoO_2$: A First Principles Study. *Chem. Mater.* **2009**, *21*, 3799−3809.

(26) Reimers, J. N.; Dan, J. R. Electrochemical and in Situ X-ray Diffraction Studies of Lithium Intercalation in Li_xCoO_2. *J. Electrochem. Soc.* **1992**, *139*, 2091−2097.

(27) Ohzuku, T.; Ueda, A. Solid-State Redox Reactions of LiCoO (R3m) for 4 V Secondary Lithium Cells. *J. Electrochem. Soc.* **1994**, *141*, 2972−2977.

(28) Matsui, M.; Dokko, K.; Kanamura, K. Dynamic Behavior of Surface Film on $LiCoO_2$ Thin Film Electrode. *J. Power Sources* **2008**, *177*, 184−193.

(29) Funabiki, A.; Inagba, M.; Ogumi, Z.; Yasuda, S.; Otsuji, J.; Tasaka, A. Impedance Study on the Electrochemical Lithium Intercalation into Natural Graphite Powder. *J. Electrochem. Soc.* **1988**, *145*, 172−178.

(30) Hirayama, M.; Sakamoto, K.; Hiraide, T.; Mori, D.; Yamada, A.; Kanno, R.; Sonoyama, N.; Tamura, K.; Mizuki, J. Characterization of Electrode/Electrolyte Interface Using in Situ X-ray Reflectometry and $LiNi_{0.8}Co_{0.2}O_2$ Epitaxial Film Electrode Synthesized by Pulsed Laser Deposition Method. *Electrochim. Acta* **2007**, *53*, 871−881.

(31) Honders, A.; der Kinderen, J. M.; van Heeren, A. H.; de Wit, J. H. W.; Broers, G. H. J. Bounded Diffusion in Solid Solution Electrode Powder Compacts. Part II. The Simultaneous Measurement of the Chemical Diffusion Coefficient and the Thermodynamic Factor in Li_xTiS_2 and Li_xCoO_2. *Solid State Ionics* **1985**, *15*, 265−276.

(32) Thomas, M. G. S. R.; Bruce, P. G.; Goodenough, J. B. Lithium Mobility in the Layered Oxide $Li_{1-x}CoO_2$. *Solid State Ionics* **1985**, *17*, 13−19.

(33) Choi, Y.-M.; Pyun, S.-I.; Bae, J. −S; Moon, S.-I. Effects of Lithium Content on the Electrochemical Lithium Intercalation Reaction into $LiNiO_2$ and $LiCoO_2$ Electrodes. *J. Power Sources* **1995**, *56*, 25−30.

(34) Aurbach, D.; Levi, M. D.; Levi, E.; Teller, H.; Markovsky, B.; Salitra, G.; Heider, U.; Heider, L. Common Electroanalytical Behavior of Li Intercalation Processes into Graphite and Transition Metal Oxides. *J. Electrochem. Soc.* **1998**, *145*, 3024−3034.

(35) Dokko, K.; Mohamedi, M.; Fujita, Y.; Itoh, T.; Nishizawa, M.; Umeda, M.; Uchida, I. Kinetic Characterization of Single Particles of $LiCoO_2$ by AC Impedance and Potential Step Methods. *J. Electrochem. Soc.* **2001**, *148*, A422−A426.

(36) Ho, C.; Raistrick, I. D.; Huggins, R. A. Application of A-C Techniques to the Study of Lithium Diffusion in Tungsten Trioxide Thin Films. *J. Electrochem. Soc.* **1980**, *127*, 343−350.

(37) Xia, H.; Lu, L.; Ceder, G. Li Diffusion in $LiCoO_2$ Thin Films Prepared by Pulsed Laser Deposition. *J. Power Sources* **2006**, *159*, 1422−1427.

(38) Jang, Y.-I.; Newdecker, B. J.; Dudney, N. J. Lithium Diffusion in Li_xCoO_2 ($0.45 < x < 0.7$) Intercalation Cathodes. *Electrochem. Solid-State Lett.* **2001**, *4*, A74−A77.

(39) Xia, H.; Lu, L.; Meng, Y. S.; Ceder, G. Phase Transitions and High-Voltage Electrochemical Behavior of $LiCoO_2$ Thin Films Grown by Pulsed Laser Deposition. *J. Electrochem. Soc.* **2007**, *154*, A337−A342.

(40) Nuspl, G.; Nagaoka, M.; Yoshizawa, K.; Mohri, F.; Yamabe, T. Lithium Diffusion in Li_xCoO_2 Electrode Materials. *Bull. Chem. Soc. Jpn.* **1998**, *71*, 2259−2265.

DOI: 10.1021/am508512q
ACS Appl. Mater. Interfaces 2015, 7, 7901−7911

(41) Catti, M. Ab Initio Study of Li^+ Diffusion Paths in the Monoclinic $Li_{0.5}CoO_2$ Intercalate. *Phys. Rev. B* **2000**, *61*, 1795−1803.

DOI: 10.1021/am508512q
ACS Appl. Mater. Interfaces 2015, 7, 7901−7911